JCI insight

RESEARCH ARTICLE

Inflammescent CX3CR1$^+$CD57$^+$CD8$^+$ T cells are generated and expanded by IL-15

Stephen R. Morris,[1,2] Bonnie Chen,[1] Joseph C. Mudd,[3] Soumya Panigrahi,[1] Carey L. Shive,[2] Scott F. Sieg,[1] Cheryl M. Cameron,[4] David A. Zidar,[2] Nicholas T. Funderburg,[5] Souheil-Antoine Younes,[1] Benigno Rodriguez,[1] Sara Gianella,[6] Michael M. Lederman,[1] and Michael L. Freeman[1]

[1]Center for AIDS Research, Division of Infectious Diseases and HIV Medicine, Department of Medicine, Case Western Reserve University/University Hospitals Cleveland Medical Center, Cleveland, Ohio, USA. [2]Louis Stokes Cleveland VA Medical Center, Cleveland, Ohio, USA. [3]Barrier Immunity Section, Laboratory of Viral Diseases, Division of Intramural Research, National Institute of Allergy and Infectious Diseases, NIH, Bethesda, Maryland, USA. [4]Center for AIDS Research, Department of Nutrition, Case Western Reserve University, Cleveland, Ohio, USA. [5]Division of Medical Laboratory Science, School of Health and Rehabilitation Sciences, Ohio State University, Columbus, Ohio, USA. [6]Center for AIDS Research, Division of Infectious Diseases and Global Public Health, Department of Medicine, University of California, San Diego, La Jolla, California, USA.

HIV infection is associated with an increase in the proportion of activated CD8$^+$ memory T cells (Tmem) that express CX3CR1, but how these cells are generated and maintained in vivo is unclear. We demonstrate that increased CX3CR1 expression on CD8$^+$ Tmem in people living with HIV (PLWH) is dependent on coinfection with human CMV, and CX3CR1$^+$CD8$^+$ Tmem are enriched for a putatively immunosenescent CD57$^+$CD28$^-$ phenotype. The cytokine IL-15 promotes the phenotype, survival, and proliferation of CX3CR1$^+$CD57$^+$CD8$^+$ Tmem in vitro, whereas T cell receptor stimulation leads to their death. IL-15–driven survival is dependent on STAT5 and Bcl-2 activity, and IL-15–induced proliferation requires STAT5 and mTORC1. Thus, we identify mechanistic pathways that could explain how "inflammescent" CX3CR1$^+$CD57$^+$ CD8$^+$ Tmem dominate the overall memory T cell pool in CMV-seropositive PLWH and that support reevaluation of immune senescence as a nonproliferative dead end.

Introduction

High expression of the fractalkine receptor (CX3CR1) on CD8$^+$ T cells identifies a population of long-lived effector memory cells with lytic granules and cytolytic capacity (1–3) that do not recirculate through lymphatics (4). Cytolytic CD8$^+$ memory T cells (Tmem) also have shortened telomeres and impaired proliferative responses to antigen — a condition termed immune senescence, characterized by high expression of CD57 and low expression of the costimulatory receptor CD28 (5–7). CD57$^+$CD28$^-$ CD8$^+$ T cells are enriched in patients with chronic viral infections, such as HIV and CMV, and are particularly enriched in people with HIV/CMV coinfection (8, 9), who comprise greater than 90% of those infected with HIV (10, 11).

In people living with HIV infection (PLWH), increased CD8$^+$ T cell numbers with resultant CD4/CD8 inversion are strongly linked to the development of non-AIDS comorbidities (12, 13). When HIV replication is controlled by antiretroviral therapy (ART), CD4$^+$ T cell numbers often recover to near normal levels, but persistently elevated CD8$^+$ T cell numbers maintain a low CD4/CD8 ratio (14). CD8$^+$ T cell expansion is likely driven by several factors, including proinflammatory cytokines such as IL-15, which is elevated during chronic HIV infection (15, 16). We recently showed that CD8$^+$ T cell expansion in ART-treated PLWH is linked to CMV coinfection (17). Many of the expanded CD8$^+$ T cells are likely to be CMV reactive (1, 18–20), be cytolytic (3, 21), and express CX3CR1 (22, 23), but what drives the sustained numbers of circulating CD8$^+$ T cells with ostensibly poor replicative capacity is not well understood.

Here we characterized peripheral blood CD8$^+$ T cells in PLWH. The majority of CX3CR1$^+$CD8$^+$ Tmem are CD57$^+$CD28$^-$ cells and are highly enriched in CMV-seropositive (CMV$^+$) donors. These cells have high expression of the transcription factor T-bet and the cytolytic enzymes granzyme B and

Conflict of interest: NTF serves as a consultant for Gilead.

Submitted: August 23, 2019
Accepted: April 30, 2020
Published: May 5, 2020.

Reference information: *JCI Insight*. 2020;5(11):e132963. https://doi.org/10.1172/jci.insight.132963.

perforin, and so are poised for effector function. In vitro IL-15 exposure promoted the development of the CX3CR1$^+$CD57$^+$ phenotype, induced the proliferation of CX3CR1$^+$CD57$^+$CD8$^+$ T cells, and sustained their viability. IL-15–induced proliferation required STAT5 phosphorylation and mTORC1 signaling, whereas IL-15–enhanced viability required phosphorylation of STAT5 and Bcl-2 activity. Thus, our data call into question the premise of immune senescence in this durably expanded cell population and provide a mechanistic link between inflammation and the expansion, activation, and persistence of CX3CR1$^+$CD8$^+$ T cells in ART-treated HIV infection.

Results

CX3CR1$^+$CD8$^+$ T cells are mostly CD57$^+$CD28$^-$ and are enriched in CMV$^+$ PLWH. Earlier, we characterized a population of CCR7$^-$CX3CR1$^+$CD8$^+$ Tmem that is enriched in the peripheral blood of ART-treated HIV-infected individuals (23). We demonstrated that CMV coinfection was necessary for CD8$^+$ T cell expansion in PLWH (17). Here, we found that CCR7$^-$CX3CR1$^+$CD8$^+$ Tmem were significantly expanded in CMV$^+$ PLWH (Figure 1A). Consistent with previous reports (1, 24), we found that a majority of CMV pp65-specific cells expressed CX3CR1, and pp65-specific cells were enriched among CCR7$^-$ cells that expressed CX3CR1 (Supplemental Figure 1A; supplemental material available online with this article; https://doi.org/10.1172/jci.insight.132963DS1). This was not seen among HIV gag-specific CD8$^+$ T cells (Supplemental Figure 1B). Regardless of CMV serostatus, however, CCR7$^-$CX3CR1$^+$CD8$^+$ Tmem were enriched for CD57$^+$CD28$^-$ cells (Figure 1B). CMV$^+$ PLWH donors also had an elevated proportion of CX3CR1^{hi}CD27$^-$CD8$^+$ Tmem (Supplemental Figure 1C) that are thought to be retained in circulation (2, 4, 24). Given that CX3CR1$^+$CD57$^+$CD28$^-$CD8$^+$ Tmem had the highest CX3CR1 density (Supplemental Figure 1D), CX3CR1^{hi} cells and CX3CR1$^+$CD57$^+$CD28$^-$ cells appeared to be largely the same population.

We next asked whether HIV infection was necessary to generate the CX3CR1$^+$CD57$^+$CD28$^-$ phenotype on CD8$^+$ Tmem. This was not the case, as CX3CR1$^+$CD57$^+$CD28$^-$CD8$^+$ Tmem were expanded in HIV-uninfected CMV$^+$ donors when compared with findings among HIV-negative, CMV-seronegative (CMV$^-$) donors (Figure 1C). Using t-stochastic neighbor embedding (t-SNE) analysis of CD8$^+$ T cells from HIV-uninfected and HIV-infected donors stratified by CMV serostatus (Figure 1D), we found that CX3CR1$^+$CD57$^+$CD28$^-$ Tmem were enriched in CD8$^+$ T cells from CMV$^+$ donors, regardless of HIV infection status, demonstrating that CMV infection alone is sufficient to promote a relatively expanded CX3CR1$^+$CD57$^+$CD28$^-$ phenotype on CD8$^+$ Tmem.

CX3CR1$^+$CD57$^+$CD28$^-$CD8$^+$ Tmem have an effector/cytolytic cell phenotype. Among CCR7$^-$CX3CR1$^+$CD8$^+$ Tmem, CD57$^+$CD28$^-$ cells had the highest expression of the effector-phenotype transcription factor T-bet and the lowest expression of the memory-phenotype transcription factor eomesodermin (Eomes), resulting in a pro-effector T-bet^{hi}Eomes^{lo} phenotype (Supplemental Figure 2A). Consistent with previous reports (21, 25), CD57$^+$CD28$^-$ cells were enriched for the cytolytic enzymes granzyme B and perforin (Supplemental Figure 2B). In general, CX3CR1$^+$CD8$^+$ T cells have greater expression of the checkpoint receptor PD-1 than do CX3CR1$^-$CD8$^+$ T cells (23). However, among CX3CR1$^+$CD8$^+$ Tmem, CD57$^+$CD28$^-$ cells had the lowest PD-1 expression (Supplemental Figure 2C), suggesting that they are less likely to be regulated by PD-1/PD-L1 interactions, and may be distinct from the recently described transitory PD-1$^+$CX3CR1$^+$CD101$^-$TIM-3$^+$CD8$^+$ T cell population that responds to PD-1 blockade in mice (26). Since CD57$^+$CD8$^+$ Tmem lack expression of CD28, we next stimulated CD8$^+$ Tmem through the T cell receptor (TCR) without anti-CD28 costimulation and measured cytokine synthesis. CD57$^+$CD8$^+$ Tmem exhibited a significantly different cytokine profile from CD57$^-$CD8$^+$ Tmem in response to TCR stimulation in the absence of costimulation (Supplemental Figure 2D), and this differential cytokine response was characterized by elevated macrophage inflammatory protein 1β (MIP-1β) expression (Supplemental Figure 2E), especially by cells that synthesized only MIP-1β (Supplemental Figure 2F). Thus, CX3CR1$^+$CD57$^+$CD28$^-$CD8$^+$ Tmem have an effector cell transcriptional profile, are poised for cytotoxicity, and are polyfunctional, with enriched MIP-1β expression.

Given that CD57 expression is associated with shorter telomeres, increased activation-induced cell death, and poor proliferative potential in response to antigen-mediated stimulation (7, 27), we wondered how CD57$^+$CD8$^+$ Tmem accumulate and persist in CMV$^+$ PLWH. To address this, we examined CCR7$^-$CX3CR1$^+$CD8$^+$ Tmem for intracellular expression of the prosurvival factor Bcl-2 (Figure 2A) and the master transcriptional regulator c-myc (Figure 2B), which is important for stimulating cell cycle progression. Both CD57$^+$CD28$^-$ and CD57$^-$CD28$^+$ cells had similar levels of Bcl-2 and c-myc expression,

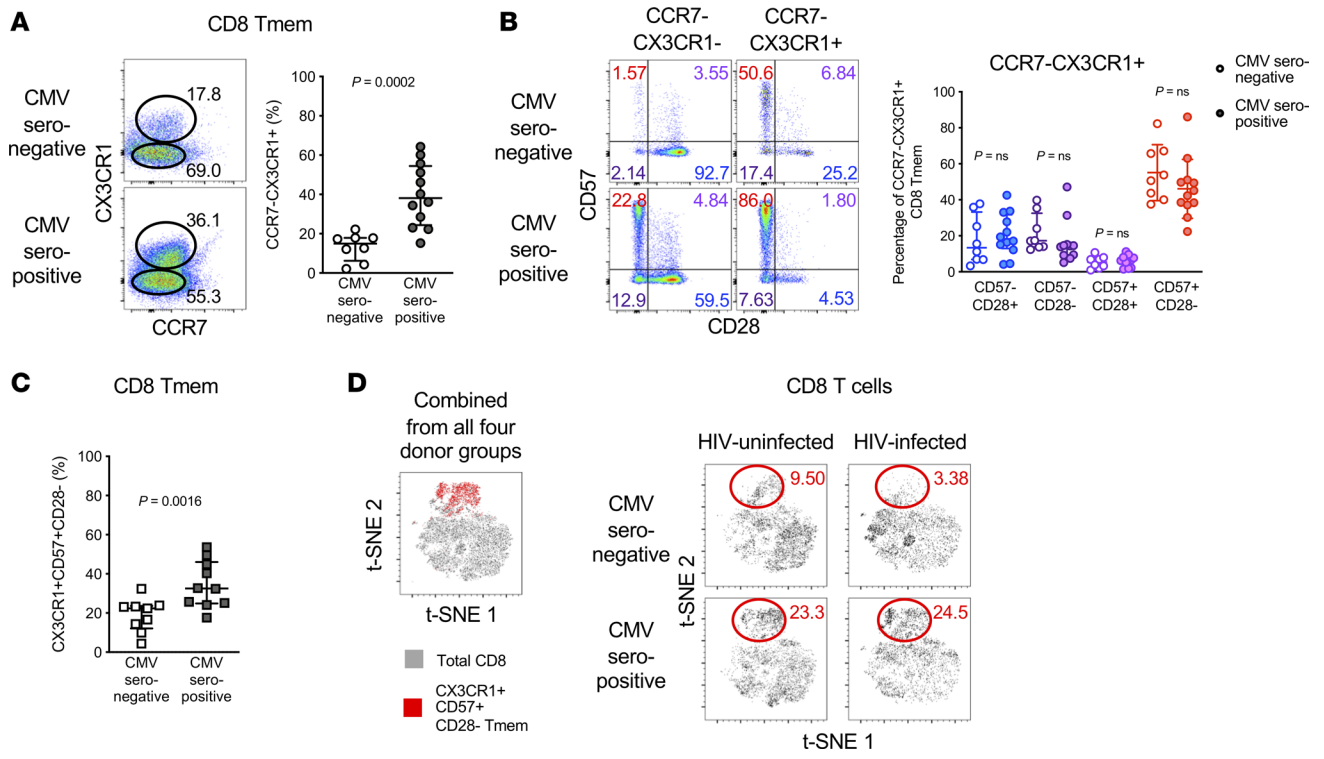

Figure 1. CX3CR1⁺CD8⁺ Tmem are expanded in HIV/CMV-coinfected individuals. Representative staining and quantification of (**A**) CX3CR1 and CCR7 expression on CD8⁺ Tmem and (**B**) CD57 and CD28 expression on CCR7⁻CX3CR1⁻ and CCR7⁻CX3CR1⁺CD8⁺ Tmem subpopulations in CMV⁻ (n = 8) and CMV⁺ (n = 12) PLWH. Data represent median ± IQR. Significance determined by Mann-Whitney U test. (**C**) Percentage of CD8⁺ Tmem that are CX3CR1⁺CD57⁺CD28⁻ in CMV⁻ (n = 9) and CMV⁺ (n = 10) HIV-uninfected donors. Data represent median ± IQR. Significance determined by Mann-Whitney U test. (**D**) t-Stochastic neighbor embedding (t-SNE) analysis of 12-parameter data of CD8⁺ T cells from combined HIV⁻CMV⁻ (n = 4), HIV⁻CMV⁺ (n = 4), HIV⁺CMV⁻ (n = 4), and HIV⁺CMV⁺ (n = 4) donors. CX3CR1⁺CD57⁺CD28⁻ Tmem are shown in red. Proportion of donor populations that are CX3CR1⁺CD57⁺CD28⁻CD8⁺ Tmem, stratified by HIV and CMV infection status.

and surprisingly, CD57⁻CD28⁻ cells had reduced Bcl-2 and c-myc levels when compared with levels in the other 2 groups — although the functional significance of these differences is currently unknown. We next measured intracellular Ki67 expression to determine the proportion of these cells actively in cell cycle. Although a lower proportion of Ki67⁺ CCR7⁻CX3CR1⁺CD8⁺ Tmem were CD57⁺CD28⁻ than among Ki67⁻ cells, the majority of CCR7⁻CX3CR1⁺CD8⁺ Tmem in cell cycle were CD57⁺CD28⁻ (Figure 2C). Taken together, our data suggest that these putatively senescent, effector-like CX3CR1⁺CD57⁺CD28⁻CD8⁺ Tmem are in cell cycle or were recently in cell cycle in vivo and are protected from apoptosis.

IL-15 promotes the generation of CX3CR1⁺CD57⁺CD8⁺ Tmem. We next asked what might be driving the generation and expansion of CX3CR1⁺CD57⁺CD28⁻CD8⁺ Tmem, with a specific focus on TCR signals and common γ chain cytokines. IL-15 exposure in particular has been shown to promote a CD57⁺CD28⁻ phenotype on CD8⁺ T cells in vitro (28, 29), enhance mitochondrial biogenesis (30), induce oxidative phosphorylation and c-myc expression (31), and promote antigen-independent proliferation without telomere loss in CD8⁺ Tmem (32, 33). In addition, our group has identified IL-15 as an important driver of bystander CD8⁺ T cell activation and expansion in chronic untreated HIV infection (15). To determine cytokine susceptibility, we measured CCR7⁻CX3CR1⁺CD8⁺ Tmem subpopulations for expression of common γ chain cytokine receptors (Supplemental Figure 3A). None of the subpopulations expressed much CD25, the α chain of the IL-2 receptor, and so were not likely to respond to low-level IL-2 exposure. All 3 subpopulations expressed robust levels of CD122, the IL-2/IL-15 receptor β chain, suggesting that they could be responsive to IL-15 or high concentrations of IL-2. There was a large variability in expression of CD127, the α chain of the IL-7 receptor; CD57⁻CD28⁺ cells often expressed CD127, whereas CD57⁺CD28⁻ cells rarely (median 11.7%) did, consistent with the more effector-like phenotype of CD57⁺CD28⁻ cells and with previous reports regarding CX3CR1^{hi}CD8⁺ Tmem (2, 34). We next stimulated PBMCs from CMV⁺ PLWH with IL-2, IL-15, or plate-bound anti-CD3 and soluble anti-CD28 mAbs (TCR) for 2 days to determine whether

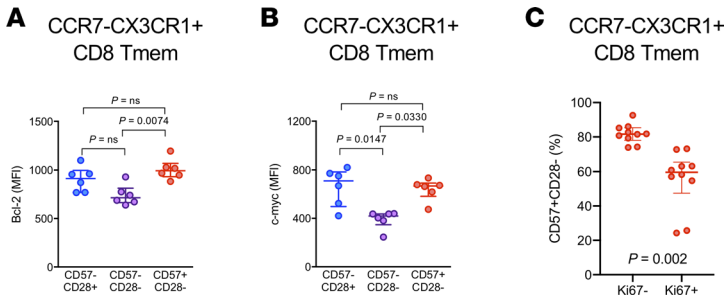

Figure 2. CX3CR1$^+$CD57$^+$CD28$^-$CD8$^+$ Tmem express Bcl-2 and c-myc and are in cell cycle in vivo. Intracellular expression of Bcl-2 (**A**) and c-myc (**B**) in subsets of CCR7$^-$CX3CR1$^+$CD8$^+$ Tmem stratified by CD57 and CD28 expression from CMV$^+$ PLWH (n = 6). Data represent median ± IQR. Significance determined by Kruskal-Wallis test with Dunn's correction for multiple comparisons. (**C**) Percentage of Ki67$^-$ and Ki67$^+$ CCR7$^-$CX3CR1$^+$CD8$^+$ Tmem that are CD57$^+$CD28$^-$ from CMV$^+$ PLWH (n = 10). Data represent median ± IQR. Significance determined by Wilcoxon's matched-pairs test.

these factors induced the CX3CR1$^+$CD57$^+$CD28$^-$ phenotype in CD8$^+$ Tmem. Treatment with IL-15 or TCR stimulation resulted in an increase in the expression of CX3CR1, but only IL-15 also sustained CD57 expression, which was downregulated on CD8$^+$ Tmem after TCR stimulation (Figure 3A), possibly due in part to activation-induced cell death of the CD57$^+$ cells. All 3 subpopulations of CCR7$^-$CX3CR1$^+$ Tmem responded to IL-15 and to TCR stimulation by increasing granzyme B and perforin coexpression (Supplemental Figure 3B). Thus, in a mixed pool of CD8$^+$ T cells, IL-15 induced expression of CX3CR1, CD57, and granzyme B and perforin, whereas TCR stimulation induced expression of CX3CR1 and granzyme B and perforin but not CD57. IL-2 had minimal effect on CD8$^+$ Tmem phenotype. To determine whether the IL-15–induced increases in CX3CR1 and CD57 reflected de novo acquisition of these molecules, we sorted CCR7$^+$CX3CR1$^-$CD57$^-$CD28$^+$CD45RO$^+$ central memory CD8$^+$ T cells (Tcm) from HIV/CMV-coinfected donors and stimulated them with IL-15 for 7 days (Figure 3B). We found a substantial increase in CX3CR1 and CD57 expression on the sorted cells, coupled with a decrease in CD28 expression. Our data therefore support the concept that the persistent accumulation of CX3CR1$^+$CD57$^+$CD8$^+$ Tmem in CMV$^+$ PLWH could be due at least in part to antigen-nonspecific mechanisms.

IL-15 promotes CX3CR1$^+$CD57$^+$CD8$^+$ Tmem viability via STAT5 and Bcl-2 activity. IL-15 has been shown to induce mitochondrial biogenesis and promote oxidative phosphorylation (OXPHOS) in T cells (30, 35). Therefore, we next measured forward scatter (i.e., cell size), mitochondrial mass, OXPHOS, and c-myc expression in stimulated CX3CR1$^+$CD57$^+$CD8$^+$ Tmem (Figure 3, C–F). Although CX3CR1$^+$CD57$^+$CD8$^+$ Tmem responded similarly to IL-15 and TCR stimulation in terms of cell size, mitochondrial biogenesis, and OXPHOS activity, only IL-15 elicited sustained c-myc expression in these cells.

CD57 expression has been proposed to mark T cells near the end of their replicative capacity (7, 27). Indeed, we found that sorted CX3CR1$^+$CD57$^+$CD28$^-$CD8$^+$ Tmem had decreased viability after 7 days of TCR stimulation (Figure 4, A and B). Conversely, viability was preserved in CD57$^+$CD28$^-$ cells by both IL-2 and IL-15. Because IL-15 promotes expression of the antiapoptosis protein Bcl-2, which supports cell survival upon activation (36, 37), we measured Bcl-2 levels after stimulation (Figure 4C). Both IL-15 treatment and TCR stimulation elicited an early upregulation of Bcl-2 levels, but only IL-15 signals durably maintained high Bcl-2 expression. Thus, our data suggest that sustained Bcl-2 expression might be required to maintain cell viability of CX3CR1$^+$CD57$^+$CD8$^+$ Tmem in the presence of the robust cell growth and mitochondrial activity induced by IL-15 and TCR signals.

To define mechanisms of IL-15–supported survival of CX3CR1$^+$CD57$^+$CD8$^+$ Tmem, we next stimulated sorted CX3CR1$^+$CD57$^+$CD28$^-$ cells with IL-15 in the presence or absence of specific inhibitors (Figures 4D and Supplemental Figure 4A). Inhibiting Bcl-2 with venetoclax reduced the viability of the sorted cells, underscoring an important role for Bcl-2 here. IL-15 signals through STAT5 to activate the nutrient sensor target of rapamycin complex 1 (mTORC1) (38), and mTORC1 is both promoted by and reciprocally promotes c-myc activity (39, 40). However, neither blocking mTORC1 activity with rapamycin nor blocking the combined activities of mTORC1 and mTORC2 with KU-0063794 affected IL-15–induced survival benefit. Blocking STAT5 phosphorylation prevented IL-15–induced survival, as did blocking Bcl-2. Thus, IL-15 promoted survival of sorted CX3CR1$^+$CD57$^+$CD28$^-$CD8$^+$ Tmem via STAT5 and Bcl-2 but independent of mTORC signaling.

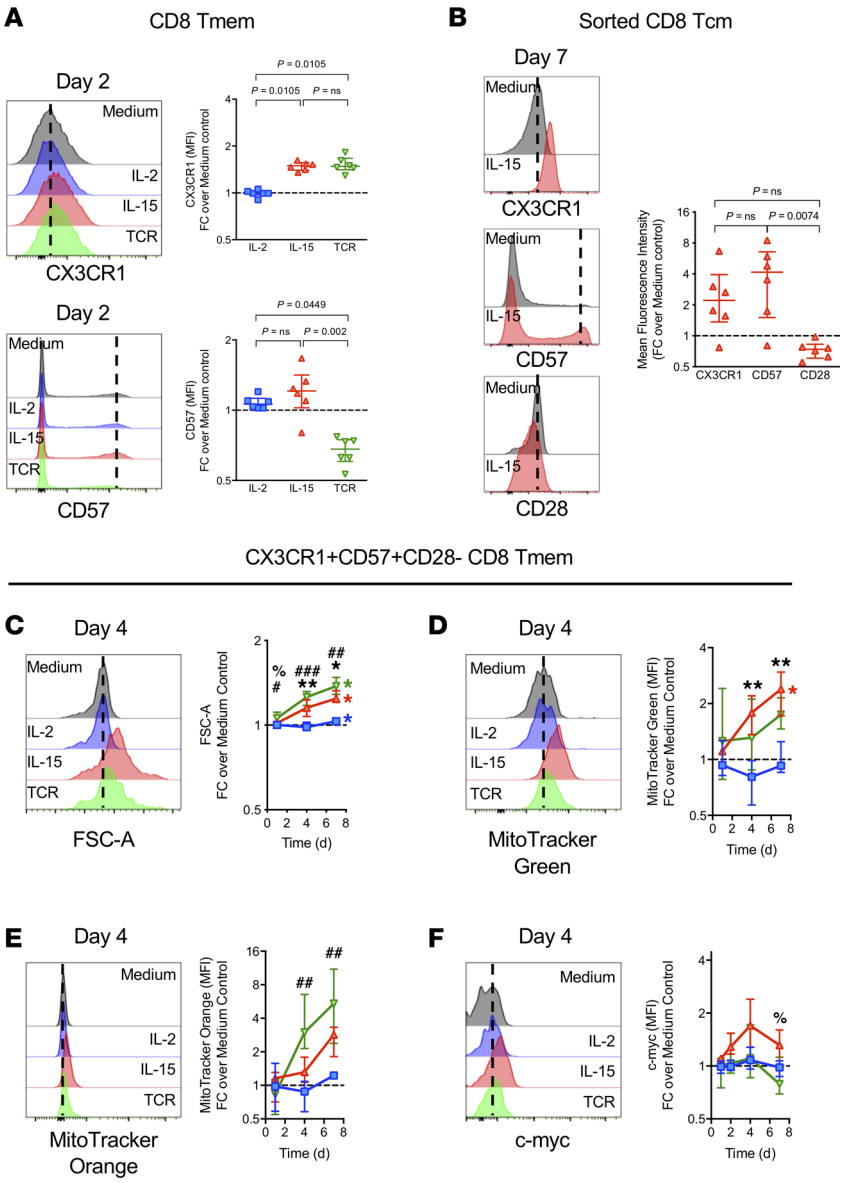

Figure 3. IL-15 promotes CX3CR1 and CD57 expression and mitochondrial activity in CD8⁺ Tmem. (**A**) Representative histograms and quantification of CX3CR1 and CD57 expression 48 hours after indicated stimulation expressed as fold change (FC) over medium control on CD8⁺ Tmem from CMV⁺ PLWH (n = 6). Data represent median ± IQR. Significance determined by Kruskal-Wallis test with Dunn's correction for multiple comparisons. (**B**) Representative histograms and quantification of CX3CR1, CD57, and CD28 expression on sorted CD8⁺ central memory T cells (Tcm) from CMV⁺ PLWH (n = 6) 7 days after IL-15 stimulation, expressed as FC over medium control. Data represent median ± IQR. Significance determined by Kruskal-Wallis test with Dunn's correction for multiple comparisons. (**C**–**F**) Representative histograms from day 4 of stimulation and quantification of forward scatter (FSC-A) (**C**), MitoTracker Green (**D**), MitoTracker Orange (**E**), and intracellular c-myc (**F**) after stimulation expressed as FC over medium control in CCR7⁻CX3CR1⁺CD57⁺CD28⁻CD8⁺ Tmem from HIV-uninfected controls (n = 7). Data represent median ± IQR. Significance among groups determined by Kruskal-Wallis test with Dunn's correction for multiple comparisons: $^{*}P \le 0.05$, $^{**}P \le 0.01$, IL-15 versus IL-2; $^{\#}P \le 0.05$, $^{\#\#}P \le 0.01$, TCR versus IL-2; $^{\%}P \le 0.05$, IL-15 versus TCR. Significance within groups (7 days vs. 1 day) determined by Wilcoxon's matched-pairs test: $^{*}P \le 0.05$.

IL-15–induced CX3CR1⁺CD57⁺CD8⁺ Tmem proliferation is dependent on STAT5 and mTORC1. Given that both IL-15 and TCR stimulation could affect cell size, c-myc expression, and mitochondrial biogenesis of CX3CR1⁺CD57⁺CD28⁻CD8⁺ Tmem, we next asked whether these exposures could drive proliferation of this reportedly senescent T cell population (Figure 5A). Because of the differences we observed in sorted cell viability after stimulation, we gated only on viable cells for proliferation analyses. IL-15 and TCR signals, but not IL-2 treatment, resulted in robust proliferation of viable cells. Because TCR stimulation did not

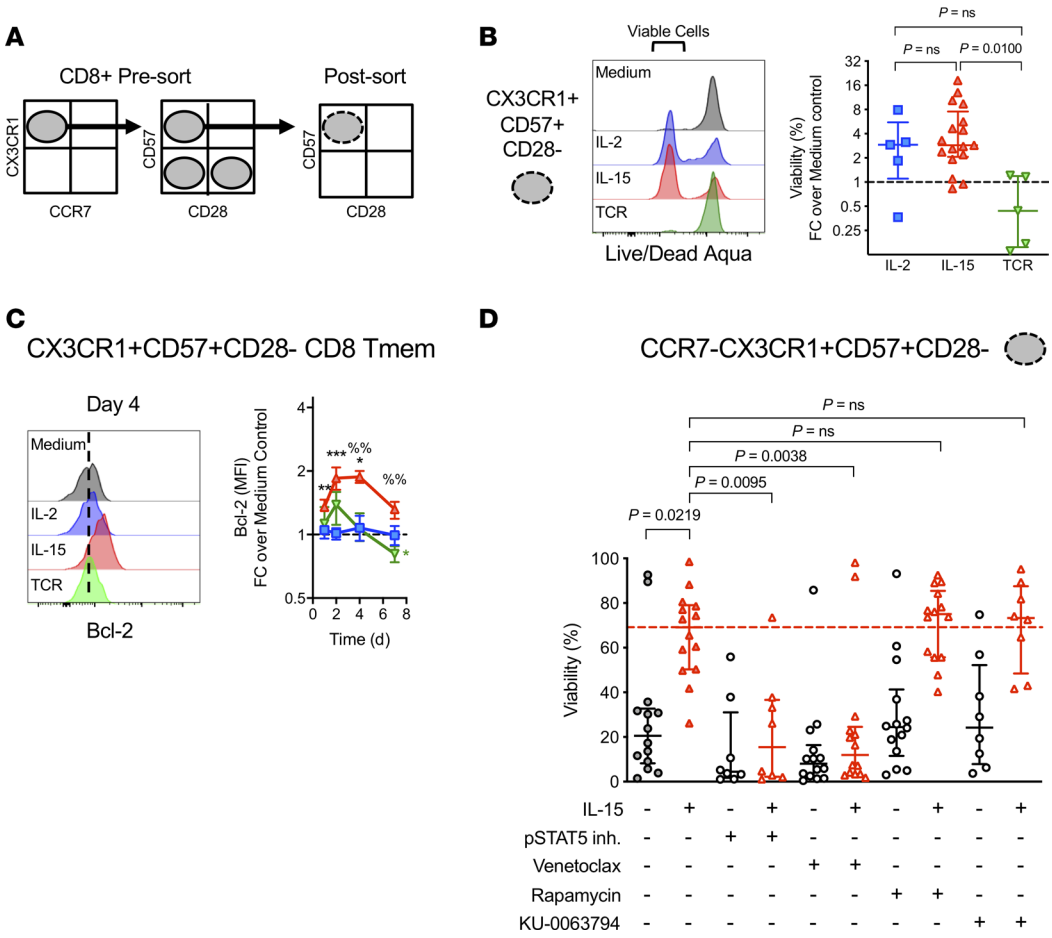

Figure 4. IL-15 promotes viability of CCR7$^-$CX3CR1$^+$CD57$^+$CD28$^-$CD8$^+$ Tmem via STAT5 and Bcl-2 activity. (**A**) Schematic of flow sorting strategy. (**B**) Representative labeling with LIVE/DEAD Aqua and quantification of viability after 7 days of stimulation expressed as FC over medium control in sorted CCR7$^-$CX3CR1$^+$CD57$^+$CD28$^-$CD8$^+$ Tmem from CMV$^+$ PLWH (n = 5–17/stim). Data represent median ± IQR. Significance determined by Kruskal-Wallis test with Dunn's correction for multiple comparisons. (**C**) Representative histograms from day 4 of stimulation and quantification of intracellular Bcl-2 staining after stimulation expressed as FC over medium control in CCR7$^-$CX3CR1$^+$CD57$^+$CD28$^-$CD8$^+$ Tmem from HIV-uninfected controls (n = 7). Data represent median ± IQR. Significance among groups determined by Kruskal-Wallis test with Dunn's correction for multiple comparisons: $^*P \le 0.05$, $^{**}P \le 0.01$, $^{***}P \le 0.005$, IL-15 versus IL-2; $^{\#\#}P \le 0.01$, TCR versus IL-2; $^{\%}P \le 0.05$, $^{\%\%}P \le 0.01$, IL-15 versus TCR. Significance within groups (7 days vs. 1 day) determined by Wilcoxon's matched-pairs test: $^*P \le 0.05$. (**D**) Viability after 7 days of stimulation with medium control or IL-15 with or without indicated inhibitors in sorted CCR7$^-$CX3CR1$^+$CD57$^+$CD28$^-$CD8$^+$ Tmem from CMV$^+$ PLWH (n = 8–14/stim). Data represent median ± IQR. Significance determined by Kruskal-Wallis test with Dunn's correction for multiple comparisons.

promote survival, and IL-2 did not drive proliferation of these cells, whereas IL-15 did both, we focused on IL-15–induced proliferation. In contrast to its impact on viability, inhibiting Bcl-2 with venetoclax did not affect proliferation induced by IL-15. However, blocking mTORC1 with either rapamycin or KU-0063794 or inhibiting STAT5 phosphorylation reduced IL-15–induced proliferation (Figure 5B and Supplemental Figure 4B). Thus, in contrast to stimulation through the TCR or exposure to IL-2, IL-15 stimulation uniquely promoted both the viability and proliferation of CX3CR1$^+$CD57$^+$CD28$^-$CD8$^+$ Tmem via STAT5 signals.

In summary, in sorted CX3CR1$^+$CD57$^+$CD28$^-$CD8$^+$ Tmem, the response to IL-15 stimulation in the absence of mTOR signals mimics the response to IL-2 treatment (enhanced viability, poor proliferation), whereas the response to IL-15 stimulation in the absence of Bcl-2 activity was similar to the response to TCR stimulation (poor viability, robust proliferation), and inhibiting STAT5 abrogated the entire IL-15 treatment response (Figure 5C). To confirm that IL-15–induced STAT5 activation was upstream of mTOR activity, we measured the phosphorylation of STAT5 and ribosomal S6 protein in CD57$^+$CD8$^+$ Tmem after 45 minutes of IL-15 exposure in the presence or absence of a STAT5 phosphorylation inhibitor or rapamycin (Figure 5D and Supplemental Figure 4C). As expected, blocking mTORC1 activity

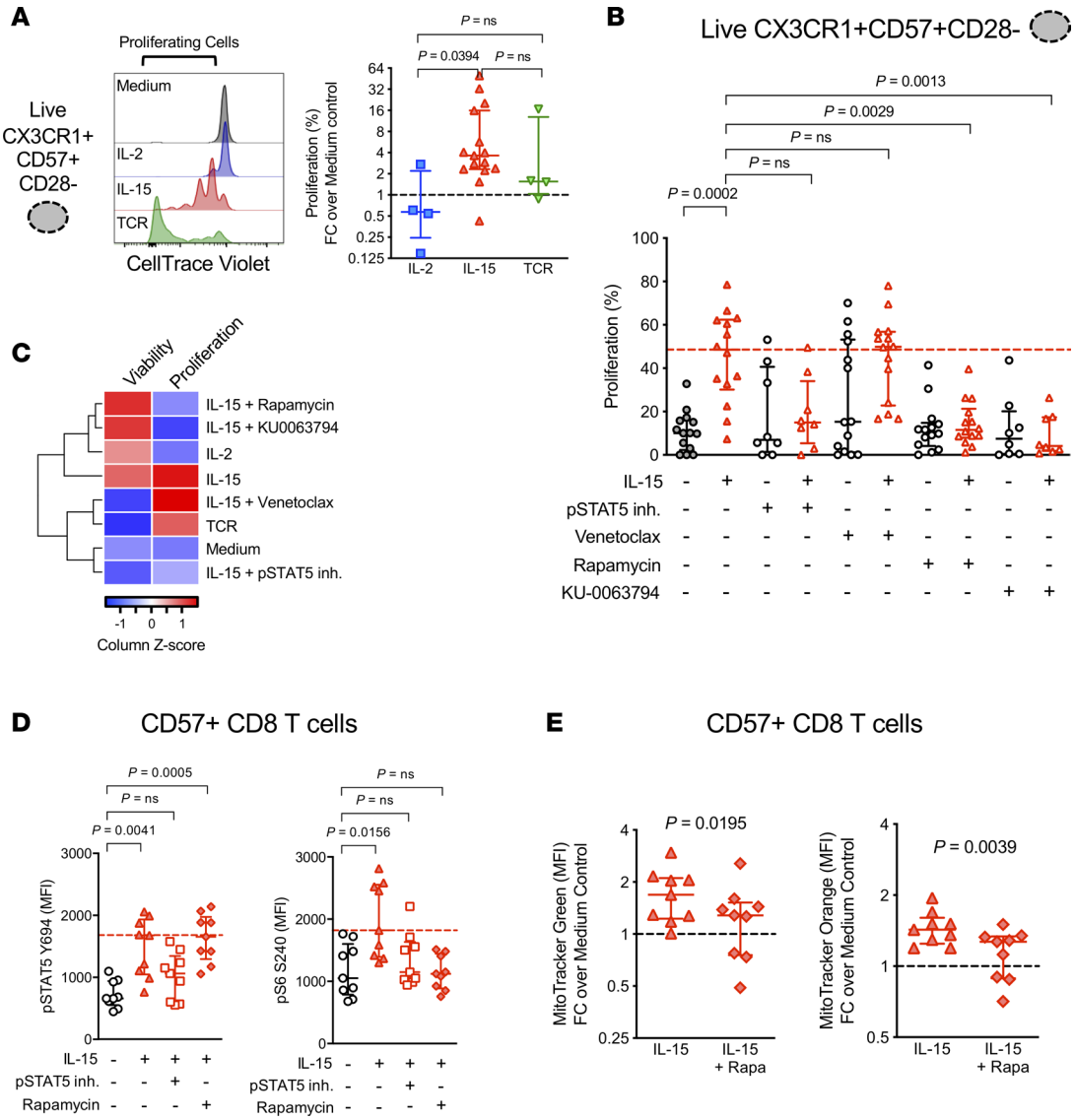

Figure 5. IL-15 promotes proliferation of CCR7$^-$CX3CR1$^+$CD57$^+$CD28$^-$CD8$^+$ Tmem via STAT5 and mTORC1 activity. (**A**) Representative labeling with CellTrace Violet and quantification of proliferation after 7 days of stimulation expressed as FC over medium control in sorted CCR7$^-$CX3CR1$^+$CD57$^+$CD28$^-$CD8$^+$ Tmem from CMV$^+$ PLWH (n = 4–15/stim), gated on viable cells. Data represent median ± IQR. Significance determined by Kruskal-Wallis test with Dunn's correction for multiple comparisons. (**B**) Proliferation after 7 days of stimulation with medium control or IL-15 with or without indicated inhibitors in sorted CCR7$^-$CX3CR1$^+$CD57$^+$CD28$^-$CD8$^+$ Tmem gated on viable cells from CMV$^+$ PLWH (n = 8–14/stim). Data represent median ± IQR. Significance determined by Kruskal-Wallis test with Dunn's correction for multiple comparisons. (**C**) Summary of viability and proliferation outcomes. (**D**) STAT5 pY694 and S6 pS240 expression 45 minutes after stimulation with medium control or IL-15 with or without indicated inhibitors in gated CD57$^+$CD8$^+$ T cells from CMV$^+$ PLWH (n = 9). Data represent median ± IQR. Significance determined by Kruskal-Wallis test with Dunn's correction for multiple comparisons. (**E**) MitoTracker Green and MitoTracker Orange labeling expressed as FC over medium control in CD57$^+$CD8$^+$ T cells from CMV$^+$ PLWH (n = 9) after 4 days stimulation with IL-15 with or without rapamycin (Rapa). Significance determined by Wilcoxon's matched-pairs test.

with rapamycin inhibited the phosphorylation of S6 but not STAT5. Blocking STAT5 phosphorylation, however, also impaired S6 phosphorylation — confirming that STAT5 activation is upstream of mTORC1 activity in IL-15–stimulated CD57$^+$CD8$^+$ Tmem. In contrast, inhibiting STAT5 phosphorylation had no effect on S6 phosphorylation in CD4$^+$ T cells stimulated with IL-15 (Supplemental Figure 4D). We next determined whether inhibiting mTOR signaling eliminated the IL-15–induced increase in mitochondrial activity. Blocking mTORC1 activity with rapamycin significantly reduced the IL-15–induced increases in mitochondrial mass and OXPHOS in CX3CR1$^+$CD57$^+$CD8$^+$ Tmem after 4 days of exposure (Figure 5E and Supplemental Figure 4E). Thus, our data suggest that IL-15 promotes proliferation of ostensibly senescent CD8$^+$ Tmem by driving mTORC1-dependent mitochondrial activity.

Discussion

The drivers and determinants of memory CD8$^+$ T cell expansion in HIV infection are incompletely described, and the distinct effects of HIV and CMV infections on CD8$^+$ Tmem phenotypes are only beginning to be understood. Recent studies have suggested that CD8$^+$ Tmem that express the vascular endothelium homing receptor CX3CR1 are an important population of cells that promote tumor and virus clearance, and that may provide a source of cells that respond to immunotherapies, such as blockade of the PD-1 pathway (1, 2, 26, 41, 42). Here, we investigated the memory CD8$^+$ T cell pool in people with or without HIV infection and found that CMV$^+$ individuals had enrichment of CX3CR1$^+$CD8$^+$ T cells that displayed surface markers of senescence (CD57$^+$CD28$^-$) and intracellular accumulation of cytolytic molecules (e.g., granzyme B and perforin), regardless of HIV infection status. These cells can be maintained and expanded in an antigen-independent manner in vitro by IL-15, via the combined activities of STAT5, Bcl-2, and mTORC1. Whereas IL-15 promoted both CX3CR1 and CD57 expression and reduced CD28 expression (43, 44), even on sorted Tcm (Figure 3B), TCR stimulation resulted in upregulation of CX3CR1 but not CD57 on CD8$^+$ Tmem in vitro (Figure 3A), suggesting that TCR stimulation drives cells toward a CX3CR1$^+$CD57$^-$CD28$^-$ phenotype. Whether CX3CR1$^+$CD57$^-$CD28$^+$ cells serve as stimulation-dependent precursors for the other 2 groups is unknown, and further study will be required to discern the developmental interactions among CX3CR1$^+$CD8$^+$ Tmem subpopulations in PLWH and in HIV-uninfected controls.

Earlier studies proposed that CD57 expression marked terminally differentiated Tmem that underwent activation-induced apoptosis in response to TCR stimulation (7, 27), and our results confirm the findings that TCR engagement results in the death of these cells. However, we showed here that terminally differentiated CX3CR1$^+$CD57$^+$CD28$^-$CD8$^+$ Tmem were capable of prolonged survival (via Bcl-2) and proliferation (via mTORC1) in response to IL-15. These effects were each dependent on the STAT5 signal transduction pathway, consistent with mechanistic studies in mice that demonstrated that antigen-independent inflammatory IL-15 stimulation of CD8$^+$ Tmem enhances cycling via STAT5 and mTORC1 (38) and survival via Bcl-2 (45). We found that IL-15 stimulates cell growth, mitochondrial biogenesis, and OXPHOS in CX3CR1$^+$CD57$^+$CD28$^-$CD8$^+$ Tmem, consistent with previous reports in CD8$^+$ and CD4$^+$ T cells (30, 35). IL-15 likely elicits these effects, at least in part, through its upregulation of c-myc, since c-myc activity is strongly linked to cell proliferation (46), mitochondrial biogenesis (47), and cell metabolism (48), and c-myc has been shown to be important for IL-15–mediated homeostatic proliferation of CD8$^+$ Tmem (31). Conversely, mTORC1 activity has also been shown to promote c-myc expression, suggesting the presence of a feed-forward loop (40, 49). Here, mTORC1 activity was necessary for the optimum induction of mitochondrial biogenesis and OXPHOS after IL-15 exposure in CX3CR1$^+$CD57$^+$CD28$^-$CD8$^+$ Tmem. IL-15 stimulation has also been shown to upregulate carnitine palmitoyltransferase 1a (Cpt1a) (30, 50, 51), a crucial rate-limiting enzyme for the β-oxidation of long-chain fatty acids (51, 52) that is downstream of c-myc (53). CD28-mediated costimulation drives Cpt1a in naive T cells primed by anti-CD3 (54), but other evidence suggests that anti-CD3/anti-CD28 may reduce Cpt1a expression (52, 55). In either case, it is possible that in the absence of CD28 costimulatory signals, TCR activation of CX3CR1$^+$CD57$^+$CD28$^-$CD8$^+$ Tmem is proapoptotic as a result of insufficient c-myc expression, dysfunctional metabolism, and a lack of Cpt1a-mediated fatty acid β-oxidation (FAO). Stimulation with IL-15, on the other hand, may promote Cpt1a expression via c-myc, leading to sustained metabolic activity and enhanced cell survival. We note, however, that a recent study showed that continuous IL-15 exposure drove less Cpt1a expression and FAO in NK cells than did intermittent IL-15 exposure (56). Whether these effects occur in IL-15–exposed CX3CR1$^+$CD57$^+$CD28$^-$CD8$^+$ Tmem, which share many functional and phenotypic attributes with NK cells, remains to be elucidated, and further research is needed to determine whether and how Cpt1a and FAO are necessary for the optimal viability of stimulated CX3CR1$^+$CD57$^+$CD28$^-$CD8$^+$ Tmem.

Recently IL-15 has been shown to be necessary for the generation and function of innate-like, virtual memory CD8$^+$ T cells (Tvm), which exhibit a memory phenotype despite never encountering specific cognate antigen, and which may provide a cross-reactive, innate-like protection from pathogens (57, 58). In humans, Tvm express a terminally differentiated Tmem phenotype (e.g., CD57$^+$), but can be distinguished from antigen-experienced terminally differentiated memory T cells by expression of killer-cell immunoglobulin-like receptors and/or NKG2A (57, 59, 60). Although we cannot exclude a contribution of Tvm to the IL-15–induced proliferation that we observed here, our preliminary data of NKG2A expression in a separate cohort of PLWH suggested that most CX3CR1$^+$CD57$^+$CD28$^-$CD8$^+$ Tmem that proliferate in response to IL-15 were presumably antigen-experienced cells (data not shown).

As the immune system ages, and as infection episodes and comorbidities accumulate, memory T cells continue to differentiate until there is an abundance of cells expressing markers associated with poor proliferative capacity, reduced life span, vascular homing potential, and robust cytotoxicity (CD57, CX3CR1, and granzyme B). CMV infection in particular appears to be a potent contributor to the generation of these cells — yet it is not clear how these terminally differentiated $CD8^+$ T cells are sustained. We show here that under conditions of inflammatory IL-15 stimulation, possibly related to CMV persistence (61), ostensibly "senescent" $CX3CR1^+CD57^+CD28^-CD8^+$ Tmem are generated, armed with effector molecules, proliferate, and retain viability in an antigen-independent manner. Our findings indicate that these highly differentiated $CD8^+$ Tmem cells are not invariably senescent and that they can be driven to proliferate when stimulated by an inflammatory cytokine — IL-15. We propose the term "inflammescent" to describe $CX3CR1^+CD57^+CD28^-CD8^+$ Tmem, which express traditional markers of senescence yet retain survival and proliferation capacities, and which are both driven by and contribute to inflammation.

Methods

Human donors and tissues. Peripheral blood was acquired in Vacutainer tubes containing EDTA (BD Biosciences) from PLWH receiving combination ART with plasma HIV RNA of less than 40 copies/mL (CMV^-, $n = 9$; CMV^+, $n = 42$) and HIV-uninfected controls ($n = 27$). Participant characteristics stratified by HIV infection status are shown in Supplemental Table 1. CMV serostatus was determined clinically by IMMULITE 2000 CMV IgG Ab immunoassay in plasma (Siemens). HIV-infected participant characteristics stratified by CMV infection status are shown in Supplemental Table 2. Although there were no significant differences between the cohorts of PLWH, we did observe trends toward more $CD8^+$ T cells and a lower CD4/CD8 ratio in the CMV^+ donors — consistent with our previous observations (17). PBMCs were purified by centrifugation over a Ficoll-Paque cushion (GE Healthcare).

Flow cytometry. Lymphocytes were identified by forward and side scatter, and phenotype was assessed using the following fluorochrome-conjugated antibodies: anti-CD3 BUV737 (UCHT1; BD Biosciences), anti-CD4 BUV395 (SK3; BD Biosciences), anti-CD8 BV605 (SK1; BD Biosciences), anti-CCR7 PE-Cy7 (3D12; BD Biosciences), anti-CX3CR1 PerCP-Cy5.5 (2A9-1; BioLegend), anti-CD25 APC-H7 (M-A251, BD Biosciences), anti-CD27 Alexa Fluor 700 (M-T271, BD Biosciences), anti-CD28 BV421 or BB515 (CD28.2; BioLegend), anti-CD45RO BV650 (UCHL1, BD Biosciences), anti-CD57 Alexa Fluor 647 or Pacific Blue (HNK-1; BioLegend), anti-CD69 PE-CF594 (FN50; BD Biosciences), anti-CD95 APC/Fire 750 (DX2, BioLegend), anti-CD101 PE (BB27, BioLegend), anti-CD122 APC (TU27, BioLegend), anti-CD127 PE (HIL-7R-M21, BD Biosciences), anti-CD244 PE-CF594 (2-69, BD Biosciences), anti–PD-1 BV786 (EH12.1, BD Biosciences), anti-SLAMF6 Alexa Fluor 647 (292811, BD Biosciences), and anti–TIM-3 BV711 (F38-2E2, BioLegend). Cells were stained for 20 minutes in the dark at room temperature, washed, and fixed in PBS containing 1% paraformaldehyde. Viable cells were gated using LIVE/DEAD Aqua viability dye (Invitrogen) per the manufacturer's instructions. For detection of intracellular molecules, after LIVE/DEAD and surface staining, cells were fixed and permeabilized with Cytofix/Cytoperm (BD Biosciences) for 20 minutes on ice and stained for 40 minutes on ice or overnight at –4°C with anti-Ki67 PE-Cy7 (B56, BD Biosciences), anti–c-myc PE (9E10, R&D Systems), anti–Bcl-2 FITC (Bcl-2/100, BD Biosciences), T-bet PE (4B10, eBioscience, Thermo Fisher Scientific), Eomes FITC (WD1928, eBioscience, Thermo Fisher Scientific), anti–granzyme B FITC (GB11; BD Biosciences), and anti-perforin PE (B-D48; BioLegend). For detection of intracellular phosphorylated proteins, cells were fixed with 16% formaldehyde for 10 minutes at 37°C, then washed and treated with 90% methanol for 20 minutes at –20°C, then washed and incubated for 20 minutes with anti-STAT5 pY694 PE (47/Stat5[pY694], BD Biosciences) and anti-S6 p240 APC (REA420, Miltenyi Biotec). To identify CMV or HIV antigen specificity, PBMCs were incubated with BV421-conjugated MHC class I HLA-A*02-restricted CMV pp65 (NLVPMVATV) or HIV gag (SLYNTVATL) peptide tetramers (NIH Tetramer Facility) for 1 hour at room temperature before surface antibody staining. Mitochondrial mass was determined by labeling cells with MitoTracker Green dye (Molecular Probes, Thermo Fisher Scientific), and mitochondrial oxidative phosphorylation activity was determined using MitoTracker Orange dye (Molecular Probes, Thermo Fisher Scientific) per the manufacturer's instructions. Tmem were determined phenotypically by excluding phenotypically naive ($CD45RO^-CCR7^+$) cells. High-dimensionality t-SNE analysis was performed using 12 parameters: CCR7, CD27, CD28, CD45RO, CD57, CD95, CD101, CD244, CX3CR1, PD-1, SLAMF6, and TIM-3. For some experiments, $CD8^+$ T cells enriched by magnetic beads (AutoMACS, Miltenyi Biotec) were then antibody labeled and sorted into subpopulations ($CCR7^-CX3CR1^+CD57^+CD28^-$, $CCR7^-CX3CR1^+CD57^-CD28^-$, $CCR7^-CX3CR1^+CD57^-CD28^+$, or $CCR7^+CX3CR1^-CD57^-CD28^+$; average

sort purity 89.4%) using a FACSAria (BD Biosciences) or S3 sorter (Bio-Rad). All flow cytometry data were acquired on an LSRFortessa flow cytometer (BD Biosciences), and analysis, including t-SNE, was performed using FlowJo software (BD Biosciences).

T cell stimulation assays. PBMCs or sorted $CD8^+$ T cell subpopulations were treated for 45 minutes (phosflow assay), or 1, 2, 4, and 7 days with medium control, recombinant IL-2 (100 U/mL; Novartis), recombinant IL-15 (20 ng/mL; R&D Systems), or anti-CD3 (10 μg/mL; HIT3a, BD Biosciences) and anti-CD28 (5 μg/mL; CD28.2, BD Biosciences). After treatment, T cells were immunostained and analyzed by flow cytometry. In some experiments, cells were labeled with CellTrace Violet (Molecular Probes, Thermo Fisher Scientific) per the manufacturer's instructions before culture to measure proliferation. Determination of proliferation precursor frequency (percentage divided) was done using FlowJo software. In other assays, cells were treated with rapamycin (250 ng/mL, MilliporeSigma), KU-0063794 (500 nM, SelleckChem), venetoclax (500 nM, SelleckChem), or N′-((4-Oxo-4H-chromen-3-yl)methylene) nicotinohydrazide (500 μM, MilliporeSigma), an inhibitor of STAT5 activity. For intracellular cytokine staining, PBMCs were stimulated with plate-bound anti-CD3 (10 μg/mL; HIT3a, BD Biosciences) or medium control in the presence of brefeldin A (GolgiPlug, BD Biosciences). After 6 hours, cells were harvested, washed, labeled with LIVE/DEAD and surface antibody, and permeabilized as above. Cells were then stained with anti–IFN-γ FITC (B27, BD Biosciences), anti–IL-2 PE-CF594 (5344.111, BD Biosciences), anti–MIP-1β PE (D21-1351, BD Biosciences), and anti-TNF APC (Mab11, BD Biosciences) for 40 minutes on ice.

Statistics. Comparisons between unrelated groups used nonparametric 2-tailed Mann-Whitney *U* tests. Comparisons among 3 or more groups were performed with nonparametric Kruskal-Wallis tests with Dunn's multiple-comparison posttests. If data passed the D'Agostino-Pearson omnibus normality test, then multiple groups were compared by 1-way ANOVA. Contingency analyses used the Fisher exact test. Paired group analyses used the Wilcoxon matched-pairs signed rank test. All statistics were performed using Prism software (version 6 or 8, GraphPad). Significance thresholds were set at P values less than 0.05.

Study approval. All human experiments were approved by the Institutional Review Board of University Hospitals, Cleveland Medical Center (protocol 01-98-55). Blood samples were acquired with written informed consent and in accordance with the Declaration of Helsinki.

Author contributions

SRM designed, performed, and analyzed experiments, and wrote the manuscript. BC, JCM, and SP performed and analyzed experiments. CLS, SFS, CMC, DAZ, NTF, and SAY provided reagents and materials, and contributed to the study design and analysis. BR and SG provided patient samples and contributed to the study design. MML provided patient samples, contributed to study design and analysis, and helped to write the manuscript. MLF conceived the study design, performed and analyzed experiments, wrote the manuscript, and guided the project. All authors reviewed and approved the manuscript.

Acknowledgments

The authors thank Brian Ferrari of the Case Western Reserve University (CWRU) Center for AIDS Research (CFAR) Immune Function Core for help with cell sorting. This work was supported by a Career Development Award (51K2CX001471-03) from the US Department of Veterans Affairs to CLS; NIH grant HL134544 to NTF; the San Diego Primary Infection Resource Consortium (NIH AI106039) and the Translational Virology Core at the San Diego Center for AIDS Research (AI036214) to SG; NIH grants (AI076174, AI069501) and the Richard J. Fasenmyer Foundation awarded to MML; and CWRU CFAR Catalytic and Developmental Awards (AI036219) to MLF.

Address correspondence to: Michael L. Freeman, 2109 Adelbert Road, BRB 1034, Cleveland, Ohio 44106, USA. Phone: 216.368.1260; Email: MLF62@case.edu.

SRM's present address is: Department of Infectious Diseases, Jackson Memorial Hospital, Miami, Florida, USA.

JCM's present address is: Division of Immunology, Tulane National Primate Research Center, Covington, Louisiana, USA.

1. Böttcher JP, et al. Functional classification of memory CD8(+) T cells by CX3CR1 expression. *Nat Commun*. 2015;6:8306.
2. Gerlach C, et al. The chemokine receptor CX3CR1 defines three antigen-experienced CD8 T cell subsets with distinct roles in immune surveillance and homeostasis. *Immunity*. 2016;45(6):1270–1284.
3. Nishimura M, et al. Dual functions of fractalkine/CX3C ligand 1 in trafficking of perforin$^+$/granzyme B$^+$ cytotoxic effector lymphocytes that are defined by CX3CR1 expression. *J Immunol*. 2002;168(12):6173–6180.
4. Buggert M, et al. Identification and characterization of HIV-specific resident memory CD8$^+$ T cells in human lymphoid tissue. *Sci Immunol*. 2018;3(24):eaar4526.
5. Focosi D, Bestagno M, Burrone O, Petrini M. CD57$^+$ T lymphocytes and functional immune deficiency. *J Leukoc Biol*. 2010;87(1):107–116.
6. Pawelec G. Hallmarks of human "immunosenescence": adaptation or dysregulation? *Immun Ageing*. 2012;9(1):15.
7. Brenchley JM, et al. Expression of CD57 defines replicative senescence and antigen-induced apoptotic death of CD8$^+$ T cells. *Blood*. 2003;101(7):2711–2720.
8. Strioga M, Pasukoniene V, Characiejus D. CD8$^+$ CD28$^-$ and CD8$^+$ CD57$^+$ T cells and their role in health and disease. *Immunology*. 2011;134(1):17–32.
9. Lee SA, et al. Impact of HIV on CD8$^+$ T cell CD57 expression is distinct from that of CMV and aging. *PLoS One*. 2014;9(2):e89444.
10. Gianella S, Letendre S. Cytomegalovirus and HIV: a dangerous pas de deux. *J Infect Dis*. 2016;214 Suppl 2:S67–S74.
11. Freeman ML, Lederman MM, Gianella S. Partners in crime: the role of cmv in immune dysregulation and clinical outcome during HIV infection. *Curr HIV/AIDS Rep*. 2016;13(1):10–19.
12. Serrano-Villar S, et al. Increased risk of serious non-AIDS-related events in HIV-infected subjects on antiretroviral therapy associated with a low CD4/CD8 ratio. *PLoS One*. 2014;9(1):e85798.
13. Serrano-Villar S, et al. HIV-infected individuals with low CD4/CD8 ratio despite effective antiretroviral therapy exhibit altered T cell subsets, heightened CD8$^+$ T cell activation, and increased risk of non-AIDS morbidity and mortality. *PLoS Pathog*. 2014;10(5):e1004078.
14. Mudd JC, Lederman MM. CD8 T cell persistence in treated HIV infection. *Curr Opin HIV AIDS*. 2014;9(5):500–505.
15. Younes SA, et al. IL-15 promotes activation and expansion of CD8$^+$ T cells in HIV-1 infection. *J Clin Invest*. 2016;126(7):2745–2756.
16. Swaminathan S, et al. Interleukin-15 (IL-15) strongly correlates with increasing HIV-1 viremia and markers of inflammation. *PLoS One*. 2016;11(11):e0167091.
17. Freeman ML, et al. CD8 T-cell expansion and inflammation linked to CMV coinfection in ART-treated HIV infection. *Clin Infect Dis*. 2016;62(3):392–396.
18. Stone SF, Price P, Khan N, Moss PA, French MA. HIV patients on antiretroviral therapy have high frequencies of CD8 T cells specific for Immediate Early protein-1 of cytomegalovirus. *AIDS*. 2005;19(6):555–562.
19. Naeger DM, et al. Cytomegalovirus-specific T cells persist at very high levels during long-term antiretroviral treatment of HIV disease. *PLoS One*. 2010;5(1):e8886.
20. Barrett L, Fudge NJ, Heath JJ, Grant MD. Cytomegalovirus immunity and exhaustive CD8$^+$ T cell proliferation in treated human immunodeficiency virus infection. *Clin Infect Dis*. 2016;62(11):1467–1468.
21. Le Priol Y, et al. High cytotoxic and specific migratory potencies of senescent CD8$^+$ CD57$^+$ cells in HIV-infected and uninfected individuals. *J Immunol*. 2006;177(8):5145–5154.
22. Combadière B, Faure S, Autran B, Debré P, Combadière C. The chemokine receptor CX3CR1 controls homing and anti-viral potencies of CD8 effector-memory T lymphocytes in HIV-infected patients. *AIDS*. 2003;17(9):1279–1290.
23. Mudd JC, et al. Inflammatory function of CX3CR1$^+$ CD8$^+$ T cells in treated HIV infection is modulated by platelet interactions. *J Infect Dis*. 2016;214(12):1808–1816.
24. Gordon CL, et al. Induction and maintenance of CX3CR1-intermediate peripheral memory CD8$^+$ T cells by persistent viruses and vaccines. *Cell Rep*. 2018;23(3):768–782.
25. Pera A, Vasudev A, Tan C, Kared H, Solana R, Larbi A. CMV induces expansion of highly polyfunctional CD4$^+$ T cell subset coexpressing CD57 and CD154. *J Leukoc Biol*. 2017;101(2):555–566.
26. Hudson WH, et al. Proliferating transitory T cells with an effector-like transcriptional signature emerge from PD-1$^+$ stem-like CD8$^+$ T cells during chronic infection. *Immunity*. 2019;51(6):1043–1058.e4.
27. Nicoli F, et al. The HIV-1 Tat protein affects human CD4$^+$ T-cell programing and activation, and favors the differentiation of naïve CD4$^+$ T cells. *AIDS*. 2018;32(5):575–581.
28. Hasan MS, Kallas EG, Thomas EK, Looney J, Campbell M, Evans TG. Effects of interleukin-15 on in vitro human T cell proliferation and activation. *J Interferon Cytokine Res*. 2000;20(2):119–123.
29. Setoguchi R. IL-15 boosts the function and migration of human terminally differentiated CD8$^+$ T cells by inducing a unique gene signature. *Int Immunol*. 2016;28(6):293–305.
30. van der Windt GJ, et al. Mitochondrial respiratory capacity is a critical regulator of CD8$^+$ T cell memory development. *Immunity*. 2012;36(1):68–78.
31. Bianchi T, Gasser S, Trumpp A, MacDonald HR. c-Myc acts downstream of IL-15 in the regulation of memory CD8 T-cell homeostasis. *Blood*. 2006;107(10):3992–3999.
32. Li Y, Zhi W, Wareski P, Weng NP. IL-15 activates telomerase and minimizes telomere loss and may preserve the replicative life span of memory CD8$^+$ T cells in vitro. *J Immunol*. 2005;174(7):4019–4024.
33. Wallace DL, et al. Prolonged exposure of naïve CD8$^+$ T cells to interleukin-7 or interleukin-15 stimulates proliferation without differentiation or loss of telomere length. *Immunology*. 2006;119(2):243–253.
34. Shin MS, et al. DNA methylation regulates the differential expression of CX3CR1 on human IL-7Rα^{low} and IL-7Rα^{high} effector memory CD8$^+$ T cells with distinct migratory capacities to the fractalkine. *J Immunol*. 2015;195(6):2861–2869.
35. Younes SA, et al. Cycling CD4$^+$ T cells in HIV-infected immune nonresponders have mitochondrial dysfunction. *J Clin Invest*. 2018;128(11):5083–5094.
36. Broome HE, Dargan CM, Krajewski S, Reed JC. Expression of Bcl-2, Bcl-x, and Bax after T cell activation and IL-2 withdrawal. *J Immunol*. 1995;155(5):2311–2317.

37. Adams JM, Cory S. The Bcl-2 protein family: arbiters of cell survival. *Science*. 1998;281(5381):1322–1326.
38. Richer MJ, Pewe LL, Hancox LS, Hartwig SM, Varga SM, Harty JT. Inflammatory IL-15 is required for optimal memory T cell responses. *J Clin Invest*. 2015;125(9):3477–3490.
39. Patidar M, Yadav N, Dalai SK. Interleukin 15: a key cytokine for immunotherapy. *Cytokine Growth Factor Rev*. 2016;31:49–59.
40. Verbist KC, et al. Metabolic maintenance of cell asymmetry following division in activated T lymphocytes. *Nature*. 2016;532(7599):389–393.
41. Zander R, et al. CD4$^+$ T cell help is required for the formation of a cytolytic CD8$^+$ T cell subset that protects against chronic infection and cancer. *Immunity*. 2019;51(6):1028–1042.e4.
42. Yan Y, et al. CX3CR1 identifies PD-1 therapy-responsive CD8$^+$ T cells that withstand chemotherapy during cancer chemoimmunotherapy. *JCI Insight*. 2018;3(8):97828.
43. Chiu WK, Fann M, Weng NP. Generation and growth of CD28^{null}CD8$^+$ memory T cells mediated by IL-15 and its induced cytokines. *J Immunol*. 2006;177(11):7802–7810.
44. Borthwick NJ, Lowdell M, Salmon M, Akbar AN. Loss of CD28 expression on CD8(+) T cells is induced by IL-2 receptor γ chain signalling cytokines and type I IFN, and increases susceptibility to activation-induced apoptosis. *Int Immunol*. 2000;12(7):1005–1013.
45. Baumann NS, et al. Tissue maintenance of CMV-specific inflationary memory T cells by IL-15. *PLoS Pathog*. 2018;14(4):e1006993.
46. Bretones G, Delgado MD, León J. Myc and cell cycle control. *Biochim Biophys Acta*. 2015;1849(5):506–516.
47. Morrish F, Hockenbery D. MYC and mitochondrial biogenesis. *Cold Spring Harb Perspect Med*. 2014;4(5):a014225.
48. Goetzman ES, Prochownik EV. The role for Myc in coordinating glycolysis, oxidative phosphorylation, glutaminolysis, and fatty acid metabolism in normal and neoplastic tissues. *Front Endocrinol (Lausanne)*. 2018;9:129.
49. Wall M, Poortinga G, Hannan KM, Pearson RB, Hannan RD, McArthur GA. Translational control of c-MYC by rapamycin promotes terminal myeloid differentiation. *Blood*. 2008;112(6):2305–2317.
50. van der Windt GJ, et al. CD8 memory T cells have a bioenergetic advantage that underlies their rapid recall ability. *Proc Natl Acad Sci U S A*. 2013;110(35):14336–14341.
51. Raud B, et al. Etomoxir actions on regulatory and memory T cells are independent of Cpt1a-mediated fatty acid oxidation. *Cell Metab*. 2018;28(3):504–515.e7.
52. Deberardinis RJ, Lum JJ, Thompson CB. Phosphatidylinositol 3-kinase-dependent modulation of carnitine palmitoyltransferase 1A expression regulates lipid metabolism during hematopoietic cell growth. *J Biol Chem*. 2006;281(49):37372–37380.
53. Melone MAB, Valentino A, Margarucci S, Galderisi U, Giordano A, Peluso G. The carnitine system and cancer metabolic plasticity. *Cell Death Dis*. 2018;9(2):228.
54. Klein Geltink RI, et al. Mitochondrial priming by CD28. *Cell*. 2017;171(2):385–397.e11.
55. Pollizzi KN, et al. mTORC1 and mTORC2 selectively regulate CD8$^+$ T cell differentiation. *J Clin Invest*. 2015;125(5):2090–2108.
56. Felices M, et al. Continuous treatment with IL-15 exhausts human NK cells via a metabolic defect. *JCI Insight*. 2018;3(3):96219.
57. White JT, et al. Virtual memory T cells develop and mediate bystander protective immunity in an IL-15-dependent manner. *Nat Commun*. 2016;7:11291.
58. Lin JS, Mohrs K, Szaba FM, Kummer LW, Leadbetter EA, Mohrs M. Virtual memory CD8 T cells expanded by helminth infection confer broad protection against bacterial infection. *Mucosal Immunol*. 2019;12(1):258–264.
59. Jacomet F, et al. Evidence for eomesodermin-expressing innate-like CD8(+) KIR/NKG2A(+) T cells in human adults and cord blood samples. *Eur J Immunol*. 2015;45(7):1926–1933.
60. Quinn KM, et al. Age-related decline in primary CD8$^+$ T cell responses is associated with the development of senescence in virtual memory CD8$^+$ T cells. *Cell Rep*. 2018;23(12):3512–3524.
61. Pangrazzi L, et al. Increased IL-15 production and accumulation of highly differentiated CD8$^+$ effector/memory T cells in the bone marrow of persons with cytomegalovirus. *Front Immunol*. 2017;8:715.